Numerical Simulation of Sprinkler Suppression of Rack Storage Fires

YI WANG, KARL V. MEREDITH, XIANGYANG ZHOU, PRATEEP CHATTERJEE, YIBING XIN, MARCOS CHAOS, NING REN, and SERGEY B. DOROFEEV
FM Global, Research Division
Norwood, MA 02062, USA

ABSTRACT

Fire suppression tests with ceiling sprinkler protection in a rack storage fuel configuration are simulated using a Computational Fluid Dynamics tool. The fuel is arranged in a double-row, six pallet-load wide and three-tier high (2×6×3) rack storage array. Each pallet load consists of three nested double-wall corrugated cardboard boxes surrounding a metal liner. Two types of ceiling sprinklers are used in this study: a pendent quick response sprinkler designated as K14, and an upright standard response sprinkler designated as K11.2. The tests are simulated using FireFOAM, which couples necessary sub-models for fire growth, sprinkler response, and fire suppression. Numerical results are compared with experiments for both free burn tests under a 20-MW calorimeter and sprinkler suppression tests under a 7.6 m high ceiling. For the free burn case, the model results show good quantitative agreement of heat release rates in all three phases, from ignition to fire growth and steady burning. For the suppression cases, the model reproduces the suppression effectiveness of the two sprinkler protection designs: K14 sprinklers suppress the fire rapidly with only one sprinkler activation, while with K11.2 sprinklers, both in the tests and simulation, the fire spreads to the pallets on the end of the fuel array with multiple sprinkler activations. The modeled sprinkler activation times are within the estimated experimental uncertainty following three repeat tests. Quantitative results characterizing sprinkler suppression performance obtained from the simulations, such as the actual delivered density (ADD) and water evaporation rate, are also reported.

KEYWORDS: CFD, fire modeling, fire growth, sprinkler-based suppression, industrial fire, FireFOAM, sprinkler activation, ADD

INTRODUCTION

Fire protection with automatic sprinklers is generally recognized as the most reliable and effective solution for industrial storage facilities. The design of a sprinkler protection system depends on the fire hazard, and needs to consider different sprinkler types and protection schemes. Currently, the sprinkler protection recommendations given by various fire codes and standards are developed from large-scale fire tests. However, the development of such recommendations is extremely challenging. This is due to the wide variations of fire hazards that depend on fuel type, storage configuration, storage height, ceiling clearance, among other parameters. On the other end, there is a variety of sprinklers available with different K-factor, response time index, temperature rating, orientation. In addition, different protection schemes with specific sprinkler spacing, in-rack options, and water demand area, may need to be considered. It is clearly not practical to develop every fire protection solution based on actual fire tests. The test results need to be generalized and engineering judgment has to come into play when information from fire tests is not available or possible. However, predicting the outcome of a large-scale fire test has been elusive, even for the most experienced engineers and scientists, mainly due to the complex interactions of many physical phenomena involved in water-based fire suppression. For example, the following phenomena need to be considered for fire growth of a relatively simple solid fuel: buoyancy driven turbulence, gas phase combustion, soot generation and oxidation, radiative and convective heat transfer, solid fuel heat transfer and degradation, boundary layer flow, etc. Moreover, the unique burning characteristics associated with many industrial fuels, e.g., melting of plastics and foams, and the porous nature of wood or plastic pallets, require special treatment. To include fire suppression one needs to first understand the spray characteristics of a given sprinkler, then the transport of the spray in the gas phase, and the water flow on the solid surfaces. Water interacts with every physical phenomenon related to fire growth, and consequently adds significant complexity to the problem. Therefore, it is highly desirable to have modeling tools that can help fire protection engineers to better understand fire suppression behavior, and help generalize limited test result data in order to provide more reliable fire protection solutions.

With the fast progress in the last two decades, Computational Fluid Dynamics (CFD) based fire modeling has already played an important role [1, 2], not only in understanding the fundamentals of fire and suppression dynamics, but also in many engineering applications, such as smoke transport and egress management. Relatively few numerical studies have been devoted to simulating large-scale fire growth and suppression. Although early works [3, 4] have demonstrated the usefulness of CFD models to understand such complex problem, there are many remaining issues to be solved so that CFD models can be reliably applied to fire growth and suppression simulations [1-5]. To achieve this long-term goal, the development of an open-source CFD fire model, FireFOAM [6, 7], has been pursued. FireFOAM is a Large Eddy Simulation (LES) code based on the OpenFOAM® [8] CFD tool box, featuring many advanced capabilities such as unstructured mesh treatment and massive parallelization. Several submodels specific to industrial fire applications have been developed and validated in a number of separate effect studies. These include gas phase turbulent flow and combustion [6, 9, 10], soot and radiation [11], solid pyrolysis [12], sprinkler spray characterization and transport [13, 14], and surface film flows [15, 16]. FireFOAM has been evaluated against test data ranging from intermediate-scale fire spread tests [17, 18] to a large-scale rack storage free burn [19] and suppression experiments [20].

The objective of this study is to describe the latest model developments and improvements integrated into the FireFOAM code, and to evaluate its performance against test data by modeling two industrial scale sprinkler fire suppression scenarios. The test configuration studied employs a double-row, six pallet-load wide and three-tier high (2×6×3) rack storage array. Each pallet-load consists of three nested double-wall corrugated cardboard boxes surrounding a metal liner. Two suppression scenarios with different types of sprinklers are modeled. One is based on protection with pendent quick response sprinklers (designated as K14) with K-factor of 200 lpm/bar$^{1/2}$ (14 gpm/psi$^{1/2}$), and the other with upright standard response sprinklers (designated as K11.2) with K-factor of 160 lpm/bar$^{1/2}$ (11.2 gpm/psi$^{1/2}$). In the following, we will first present major sub-models and model improvements used in the current study. Experiments carried out for the model evaluation are then described, followed by the mesh details and numerical setup. Next, model results and their comparison with experimental data are presented, followed by discussion and conclusions.

MODEL DESCRIPTION

The gas phase solver of FireFOAM [9] is designed for buoyancy driven turbulent reacting flow. Originally FireFOAM solved the standard mixture fraction and total enthalpy conservation equations. Turbulent diffusion combustion was modeled by the beta-pdf method. The transport equation of mixture fraction variance was solved. In the present work the governing equations are changed to solve the conservation equations for individual species and sensible enthalpy. The change of the governing equations is motivated by the need to track water vapor separately in the gas phase as required by the water suppression model. In addition, the new formulation of the conservation equations requires explicit modeling for the reaction and heat release rates, which provides direct output to measure fire size and makes it easier to model gas phase extinction, which is planned for future extension. A one-step, infinitely-fast, non-reversible chemical reaction scheme is assumed. For a typical hydrocarbon fuel, transport equations for the four following species are needed: fuel, O_2, H_2O, and CO_2. The mass fraction of N_2 is obtained from species conservation. Two extra equations are now solved in the new formulation compared to the previous formulation that consists of two scalars (mixture fraction and its variance). The added computational expense, however, is insignificant because the computational time is mostly consumed by solving the pressure equation and by radiation calculations.

Turbulent diffusion combustion is currently modeled by the eddy dissipation model, as follows:

$$\overline{\dot{\omega}_F} = C_{EDC}\overline{\rho}\frac{\varepsilon}{k}\min\left(\widetilde{Y}_F, \frac{\widetilde{Y}_O}{s}\right), \tag{1}$$

where $\overline{\dot{\omega}_F}$ denotes the turbulent fuel reaction rate, $\widetilde{Y}_F$ and $\widetilde{Y}_O$ are the Favre filtered mass fractions of the fuel and oxidizer respectively, s is the stoichiometric oxidizer-to-fuel ratio, $\overline{\rho}$ is the filtered density, ε is the sub-grid scale dissipation rate, k is the sub-grid scale turbulent kinetic energy, and C_{EDC} is the model constant. This combustion model assumes that the turbulent reaction rate is determined by the turbulent mixing time scale k/ε, and is dependent on the availability of fuel and oxidizer as well.

The radiative transfer equation (RTE) is solved by a finite-volume implementation of the discrete ordinate method. The optically-thin assumption is used, which is justified for the current study because the most important region for the radiative heat transfer is within narrow flue spaces and gaps between tiers. The emission source within the gas phase is assumed to originate solely from the reaction zone with a fixed fraction of the heat release rate. A 22 % constant radiant fraction is used for this study, which is an average value for the pyrolysate of the corrugated cardboard based on Ref. [21].

An empirical wall function derived from a wall-resolved LES study of vertical wall fires [22] is used in the current simulation for convective heat transfer. As shown in Ref. [22], the wall-normal grid resolution for a wall-resolved fire case should be on the order of 2 mm. For a coarser grid, a turbulent thermal diffusivity is calculated based on the ratio of mean heat flux predicted from the wall-resolved simulation to the resolved convective heat flux by the coarser mesh. The wall function also accounts for the effect of the mass transfer rate in the pyrolysis region, or so called "blowing effect" [23], that yields smaller convective heat flux in the presence of the fuel mass flux, as follows:

$$\dot{q}''_{c,pyrolysis} = \dot{q}''_{c,flame}\left[\frac{\dot{m}''/h_m}{\exp(\dot{m}''/h_m)-1}\right]. \tag{2}$$

Here, the $\dot{q}''_{c,pyrolysis}$ and $\dot{q}''_{c,flame}$ are the convective heat flux with and without mass transfer; $\dot{m}''$ is the mass flux from the fuel surface, and h_m is the mass transfer coefficient.

The pyrolysis model used in the current study follows that in Refs. [12, 17]. Several extensions have been implemented, however, i.e., char-oxidation and surface emissivity characterization. The char-oxidation model based on Ref. [24] assumes surface reaction that is controlled by oxygen diffusion. Spectral surface emissivities of the corrugated cardboard, both in its virgin and charred states, have been measured in experiments. This allows for the determination of the effective emissivity of the material, depending on the spectral radiation environment it is subjected to, and defines the boundary conditions for the pyrolysis model [18]. To obtain the material properties, the response of corrugated cardboard material is measured in bench-scale Fire Propagation Apparatus (FPA) tests under three different heat flux conditions: 25 kW/m^2, 50 kW/m^2, and 100 kW/m^2. The surface temperature, fuel mass loss rate, and the cumulative mass loss are measured and used as the objective functions to determine the parameters of the pyrolysis model through inverse modeling and optimization [12]. The optimized effective properties for double-wall corrugated cardboard are listed in Table 1.

Sprinkler activation is modeled using classical RTI correlation [25], as shown in Eq. 3.

$$\frac{dT_d}{dt} = \frac{u^{1/2}(T_g - T_d) - C(T_d - T_{\text{int}})}{RTI}, \tag{3}$$

where T_g and T_d are the temperature of the surrounding gas and the sprinkler thermal link respectively, while T_{int} is the initial temperature of the sprinkler; u is the gas velocity; RTI is the response time index; and C is a parameter to account for conductive heat loss to the sprinkler mount.

The sprinkler injection model uses empirical correlations based on experimental measurements [13-14]. Volume flux, droplet diameter distribution and velocity are calculated from fitted functions of elevation angle, with different coefficients for each azimuthal angle. The droplet transport is modeled using a Lagrangian particle tracking method. Details on transport equations for mass, momentum and energy, as well as the submodels for drag, heat and mass transfer can be found in Ref. [14].

Table 1. Optimized material properties for double-wall corrugated cardboard.

	Property	Value
Virgin	Thermal Conductivity (W/m^2/K)	0.42
	Density (kg/m^3)	183.7[a]
	Heat Capacity (J/kg/K)	2697
	Emissivity	Varies[b]
Char	Thermal Conductivity (W/m^2/K)	0.33
	Density (kg/m^3)	23.6
	Heat Capacity (J/kg/K)	1450[c]
	Emissivity	0.9[d]
Reaction	Pre-exponential Factor (s^{-1})	3.29×10^{10}
	Activation Energy (J/mol)	1.31×10^{5}
	Heat of Pyrolysis (J/kg)	2.92×10^{5}
	Reaction Order	1.26
Heat of combustion	Virgin (J/kg)[e]	16.6×10^{6}
	Char (J/kg) [f]	32.8×10^{6}
	Pyrolysate (J/kg)[g]	14.2×10^{6}

[a] Direct measurement at room temperature.
[b] Effective emissivity determined from spectral measurements [18].
[c] Heat capacity of graphite at the average temperature of interest.
[d] Prescribed value.
[e] Value measured by oxygen bomb calorimeter.
[f] Heat of combustion of carbon.
[g] Calculated from the heats of combustion of virgin and char, weighted by the char mass fraction

Sprinkler-based fire suppression mainly relies on the water flow cascading on the fuel surfaces [26-28]. This cascading water flow pre-wets and cools the fuel resulting in reduced fire spread over the surface and fuel supply rate. To this end, a comprehensive water film model [15, 16] has been developed to predict the water transport on solid surfaces. Conservation equations on a two dimensional surface are solved for the water film, assuming that the film is thin and the velocity in the surface-normal direction is negligible. The model accounts for the interfacial mass, momentum and energy transfer among the water film, spray droplets, gas phase and solid fuel. Those interactions include phenomena such as splashing, evaporation, absorption, dripping, etc. The thermal cooling of the fuel surface provided by the water flow is achieved through the blockage of radiative and convective heat transfer from the gas phase, as well as the convective cooling by the water flow. The reduced solid phase temperature due to surface cooling leads to a local reduced burning rate and to possible suppression of the burning region. Also the presence of the water film on the surface prevents flame spread to the pre-wetted areas. Details of the water film model and separate effect validations can be found in Refs. [15, 16, 20]. It is noted that gas phase extinction, another suppression mechanism that is more relevant to water mist system [28], is not considered in the current gas phase model. However, the cooling of the gas phase due to water evaporation is included in both the spray and water film models. Thus, the current suppression model captures the dominant mechanism for sprinkler-based fire suppression. It is physics based, as opposed to Refs. [3, 4], where empirical correlations for water suppression were adopted.

EXPERIMENTS

A series of large-scale experiments was carried out at the FM Global Research Campus to provide test data for model evaluation. Suppression scenarios with two types of sprinklers were tested: K14 pendent and K11.2 upright. The corresponding specifications of the two types of sprinklers are listed in Table 2. The K14 sprinkler has a faster response time, lower temperature rating, and larger discharge rate, compared to the K11.2 sprinkler. The operating pressure was set to 1.31 bar for K11.2 sprinkler tests and 3.45 bar for K14 sprinkler tests. Ceiling level sprinkler protection was provided with equal sprinkler spacing of 3.05 m.

The test configuration involves a 2×6×3 rack storage array, as shown in Fig. 1. The dimension of each box is (1.07 m)^3. The bottom tier is raised by 13 cm from the floor. The vertical spacing between tiers is 46 cm. The flue space is 15 cm in both longitudinal and transverse directions. A separate single-row target array

(1×6×3) is placed behind the main array with a 1.22 m wide aisle in between. The fuel array setup was very similar to the standard Class 2 commodity used in the commodity classification project [29], with the only difference being that the wood pallets used in the standard commodity are replaced by four metal point supports at the corners of each box. The fuel array is placed under a movable ceiling, which is set to 7.62 m above the floor so that a 3.05 m ceiling clearance from the top of the fuel array is obtained. For each test the ignition is in the center of the main fuel array at the bottom tier. The ignition source is made of four 7.6 cm diameter and 7.6 cm long igniters with cellucotton material each soaked with 59 ml of gasoline.

Six fire suppression tests were carried out, with three repeats for each of the two sprinkler scenarios. In addition, two free burn tests were carried out under a 20-MW calorimeter, where the heat release rate history can be measured. The free burn tests used a 2×4×3 fuel array, narrower than the suppression tests, due to the limitations of the calorimeter. The reduced array size, however, does not influence the early stage of the fire growth.

Table 2. Sprinkler type and parameters.

Sprinkler Name	K factor [lpm/bar$^{1/2}$]	RTI [(m·s)$^{1/2}$]	C factor [(m/s)$^{1/2}$]	Temp Rating [°C]	Pressure [bar]	Flow rate [lpm]
K11.2 upright	160	90.0	0.525	141	1.31	183
K14 pendent	200	27.6	0.692	74	3.45	371

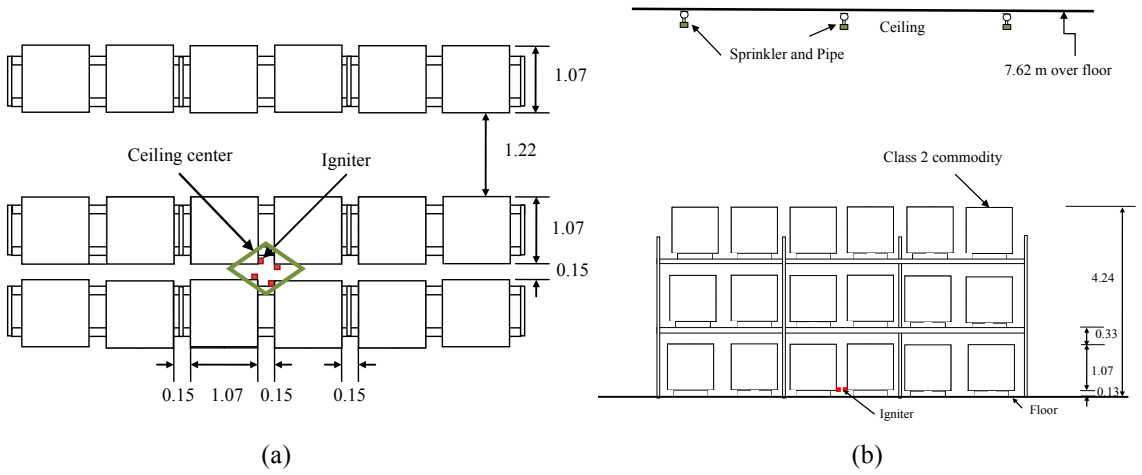

Fig. 1. Illustration of the sprinkler fire tests setup: (a) plan view, (b) elevation view (units: m).

NUMERICAL SETUP

Computational Mesh

The rectangular computational domain has dimensions of 18×18×10.2 m. Dimensions are written in the order of depth, length, and height, respectively. This same convention will be followed throughout the paper. In the fire tests, corrugated cardboard boxes are placed on a metal rack with point supports. The obstruction provided by the rack structure on the flow entrainment and flame spread is assumed to be negligible. Therefore, those details are not included in the simulations for simplification. For the same reason, the target array is treated as non-flammable material; thus, it only affects the entrainment flow pattern. A ceiling of 15 ×15 m size is included, which is smaller than the size of the actual movable ceiling (24.4×24.4 m) in the fire tests. A reduced ceiling size is used in the simulations to fit into the computational domain; however, it is not expected to affect the results of interest herein.

Nine sprinklers in a 3×3 arrangement are implemented in the numerical setup. Following the test conditions, the center sprinkler is directly above the center of the main fuel array, which is also the ignition location. In the simulation, it is assumed that the link and deflector are at the same location: for the K11.2 upright sprinkler, 0.2 m below the ceiling; and for the K14 pendent sprinkler, 0.4 m below the ceiling.

The computational mesh is created by a mesh generation utility, *snappyHexMesh*, provided in the OpenFOAM package. The *snappyHexMesh* utility generates three-dimensional meshes containing hexahedra and split-hexahedra automatically. The background Cartesian block mesh can be refined to different levels according to a preset refinement level for a certain sub-domain. In a refinement zone, each cell is split in half in the three coordinate directions, resulting in a cell volume of 1/8 compared to cells in the zone one level coarser. Split-hexahedra are created at the interface of two refinement zones. In the current simulation, the coarsest mesh has a cell size of 0.3×0.3×0.6 m. The finest refinement level is 4, which leads to the smallest cell size of 1.875×1.875×3.75 cm – yielding eight cells across the 15 cm flue space. As shown in Fig. 2, the level-4 refinement zone covers all four columns of boxes in the middle of the array, and a small portion of the outside columns. Since the flame does not considerably spread to the outside boxes in the fire tests for the time period of interest, a coarser mesh is used for those boxes to reduce the computational cost. The level-3 refinement zone (3.75×3.75×7.5 cm cell size) is used for the center plume region (2.4×2.4 m, from the top of the array to the ceiling level) and the ceiling layer region (8.4×8.4 m, 30 cm below the ceiling) where the sprinklers are located.

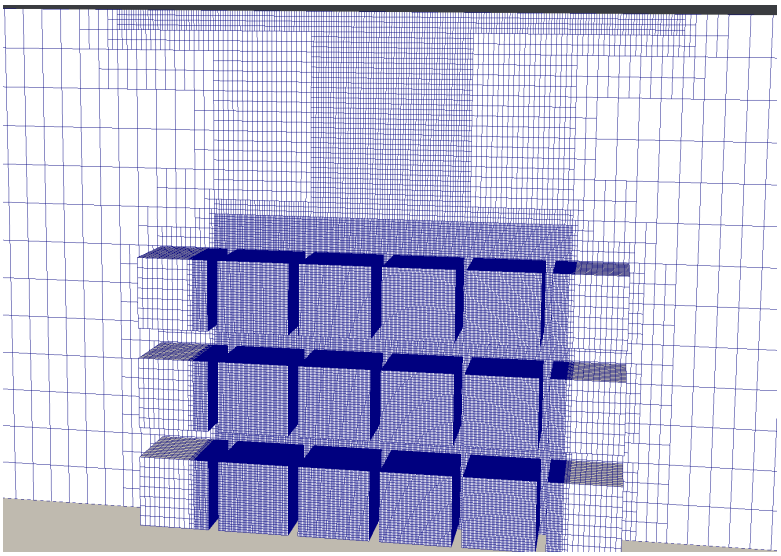

Fig. 2. Computational mesh showing refinement regions.

The total number of cells in the gas phase is 4.17 M. The flexibility of the unstructured mesh makes it possible for FireFOAM to model large industrial scales while maintaining centimeter level resolution in the region of interest. The mesh in the liquid film region is a single-layer one-cell thick mesh extruded from the surface mesh of the boxes [15, 16]. Cells in the liquid phase conform to the boundary faces in the gas phase, with a total number of cells of about 352 K. The solid phase mesh is extruded from the same face cells, and is one dimensionally perpendicular to the surface. Twenty cells are used in the direction across the material, making the total number of solid cells to be 7.04 M. The mesh for the free burn case has the same mesh refinement zone and resolution around the fuel rack, while the plume region and original ceiling region are not as refined as in the suppression cases. So the total mesh size for the free burn case is slightly smaller than for the suppression case: 3.83 M in the gas phase and 6.02 M in the solid phase.

All the simulations were carried out using 192 CPU cores in an in-house cluster with Intel® Xeon® processors (X5650, 2.67GHz) and InfiniBand network connection. The wall clock time for the free burn simulation up to 180 s of physical time was 133 hours. The Courant number was set to a value in the range of 0.6 to 0.8. For the suppression case with K11.2 sprinklers, a Courant number of 0.6 was used, taking 107 hours of wall clock time for a simulation up to 120 s of physical time.

RESULTS AND DISCUSSION

Fire Growth Modeling

While the free burn fire simulation is not the main focus of the present paper, an adequate prediction of fire growth is an important prerequisite for the sprinkler-based fire suppression modeling as it determines the

sprinkler activation time as well as the interactions of fire with spray and water film flows. Therefore, we first examine the model results for the 2×4×3 rack storage free burn fire test. Figure 3 shows a comparison of the experimental and simulated chemical heat release rate (HRR). Symbols in the figure are the HRR obtained from CO/CO_2 generation calorimetry from the two repeat fire tests. To represent the HRR in real time, the experimental data in Fig. 3 are corrected to remove the time delay that is associated with gas transport in the calorimeter duct and gas analyzer. When the fire size is smaller than 1 MW, an estimated plume transport time from the fire to the product collector hood is used to correct the initial HRR curve. When fire is larger than 1 MW, this transport time is negligible due to a higher plume velocity and the elevated fire location.

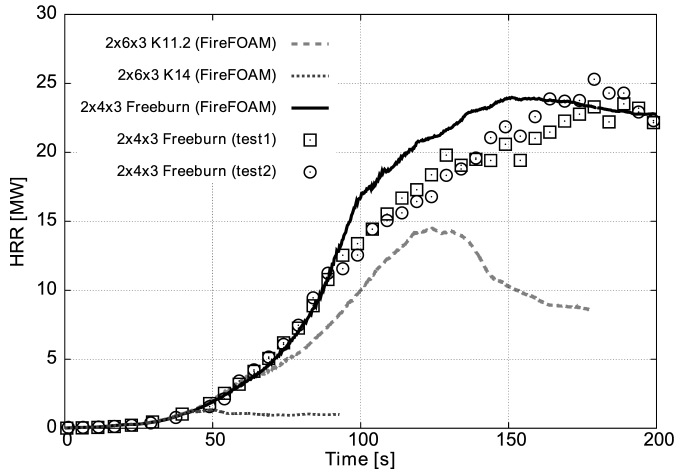

Fig. 3. Heat release rate history of free burn and sprinkler suppression fire cases.

The test data in Fig 3 show good repeatability for the fire growth history. Prior to 85 seconds, fire growth is exponential reaching an HRR of approximately 10 MW. This corresponds to the stage when the center two columns of boxes at the second and third tiers are fully engulfed in fire. From 85 to 150 s, an approximately linear growth rate is observed, and fire spreads horizontally to the outside columns causing the fire size to roughly double. The fire reaches a peak heat release rate of 23 MW at around 150 s, followed by a long steady burning period thereafter.

The modeled HRR, shown in Fig. 3 by the solid curve is calculated from the fuel mass loss rate along with the heat of combustion values shown in Table 1. This approach has been confirmed to match the domain-integrated heat release rate in the gas phase. It is seen that the modeled overall fire growth trend compares well with the experimental data. The model quantitatively reproduces the experimentally observed trends including an initial growth period leading to a peak heat release rate and followed by steady burning. In the linear growth period, the model over-predicts the heat release rate by about 10-20%. This may indicate that the model has a slightly faster horizontal flame spread when the fire propagates from the center to the outside boxes. This may also be due to the fact that the model does not describe changes in the geometry of the flue spaces and flow blockage resulting from partial delamination of the corrugated layers. Considering the uncertainties intrinsic to such a large-scale fire, this level of deviation in the time resolved HRR can be regarded as relatively low. It should also be noted that the initial stage of fire growth up to 2 MW, where the model performs well, is very critical for modeling sprinkler activation and subsequent suppression phenomena. In summary, the performance of the fire growth modeling part has shown significant improvements from the earlier studies (see e.g., [19]) due to the model improvements described in the previous section.

Fire Suppression Modeling

The simulated HRRs for a 2×6×3 rack storage with the two types of sprinklers are also plotted in Fig. 3. The time-resolved HRR is not available from experiments because the product collection above the ceiling is error prone, due to the delayed gas transport, recirculation above the ceiling, as well as the interaction of product gases with sprinkler sprays. The modeled HRRs show the dramatically different suppression effectiveness provided by the K11.2 versus K14 sprinklers. The K14 sprinkler located over ignition activates at 42 s, when the chemical HRR is about 1 MW. The early activation combined with the relatively

large water flow rate of 370 lpm (see Table 2) results in early fire suppression with only one sprinkler activated. On the other hand, the K11.2 sprinkler over the ignition location activates at 59 s. The more than ten seconds difference in activation time allows the fire in the K11.2 case to almost triple in size to 2.5 MW compared to the K14 case. The relatively small water flow rate of 180 lpm from the first activated sprinkler cannot prevent fire growth. The fire size continues to increase at a reduced rate to about 14 MW until four adjacent sprinklers activate from 117 to 126 s resulting in the reduction of the HRR.

The fire suppression behavior described above can also be confirmed visually in Fig. 4 comparing a series of experimental and numerical "snapshots" from 20 to 160 seconds, one every 20 seconds. The numerical snapshots show stoichiometric mixture fraction iso-contours. In the model visualization shots, the nine grey cones on the ceiling represent the sprinkler locations. A sprinkler is colored red as soon as it activates. The light blue dots represent water spray from sprinklers. The brightness of the light sand color on the box surfaces represents the water film thickness. Contrasting with the original darker sand color of the dry boxes, this color scheme represents the coverage patterns on the box surfaces.

For the K14 sprinkler case, after sprinkler activation, water quickly covers the entire vertical surfaces of the fuel boxes on the center two columns (referred to as "inner columns" hereafter) within twenty seconds. Fire is suppressed quickly by water without any chance of further spread. For the K11.2 case, twenty seconds after sprinkler activation (around 80s), only thin rivulets are formed on the top tier boxes as well as, partially, on the second tier boxes (see Fig. 4d). At this time, fire is mainly in the center flue space and underneath the center boxes in the second and third tiers. The rivulet flow is not able to stop fire growth in the center rows. At about 100-110 s, fire growth is sufficiently strong to dry out the partially wetted surfaces and spread out to the entire vertical faces of the boxes (Fig. 4e). At the same time, fire also spreads to the bottom faces of the top tier boxes in the columns on each side of the inner columns (Fig. 4f) (referred to as "intermediate columns" hereafter). Shortly thereafter, similar horizontal fire spread extends to the second tier as well (Figs. 4g and 4h).

Both the model and the tests show a slightly faster horizontal spread on the higher tier compared to the lower one. The sprinkler to the left of the inner columns is activated at about 117 s in the simulation (Fig. 4f), and within 10 seconds the other three sprinklers next to the center sprinkler are all activated (Fig. 4g). The increased water discharge starts to reduce fire intensity in the inner columns, with the fire plume above the rack reducing in size, as shown in Figs. 4g and 4h. Nonetheless, the fire still manages to spread further outwards to the bottom of the second tier in the intermediate columns. The same spread is also observed in the tests.

Variations exist in the three repeat tests regarding sprinkler activation times and sequence. Table 3 lists the number of activated sprinklers and the activation time for the first and second sprinklers. For all the K14 tests, only one sprinkler activated and was sufficient to suppress the fire. The activation time ranges from 40 to 50s, while the simulated activation time is 42 s. For the K11.2 tests, the first sprinkler activation time is in the range of 55-76s, and the activation time in the simulation is 59 s. It is noted that the predicted first sprinkler activation time for both suppression scenarios is within the observed experimental range. The activation time for the second sprinkler in the K11.2 tests is in the range of 97-111 s, while it is 117 s in the simulation. The reason for the slightly delayed activation may be due to many factors in the model. However, given the experimental uncertainties this difference may not be significant.

Figure 5 presents more detailed information of sprinkler activation time, sequence, and location for the K11.2 cases. The location of the second activated sprinkler seems to be somewhat random in the three tests. For test 1, it is the one directly above the left side of the main fuel array; for test 2, the one further away at the left back corner; and for test 3, the one in the center front. Even more randomness is present in the subsequent sprinkler activation time and pattern. Regardless of the randomness at later stages, there is a consistent trend in the overall fire suppression of the K11.2 tests: the first sprinkler activated around 1 minute with chemical HRR of approximately 3 MW; a single sprinkler fails to control the fire and around 40-45 seconds later, a group (2 to 6) of nearby sprinklers are activated within a short time interval and reduce the fire intensity. This behavior is indeed satisfactorily reproduced by the numerical simulation.

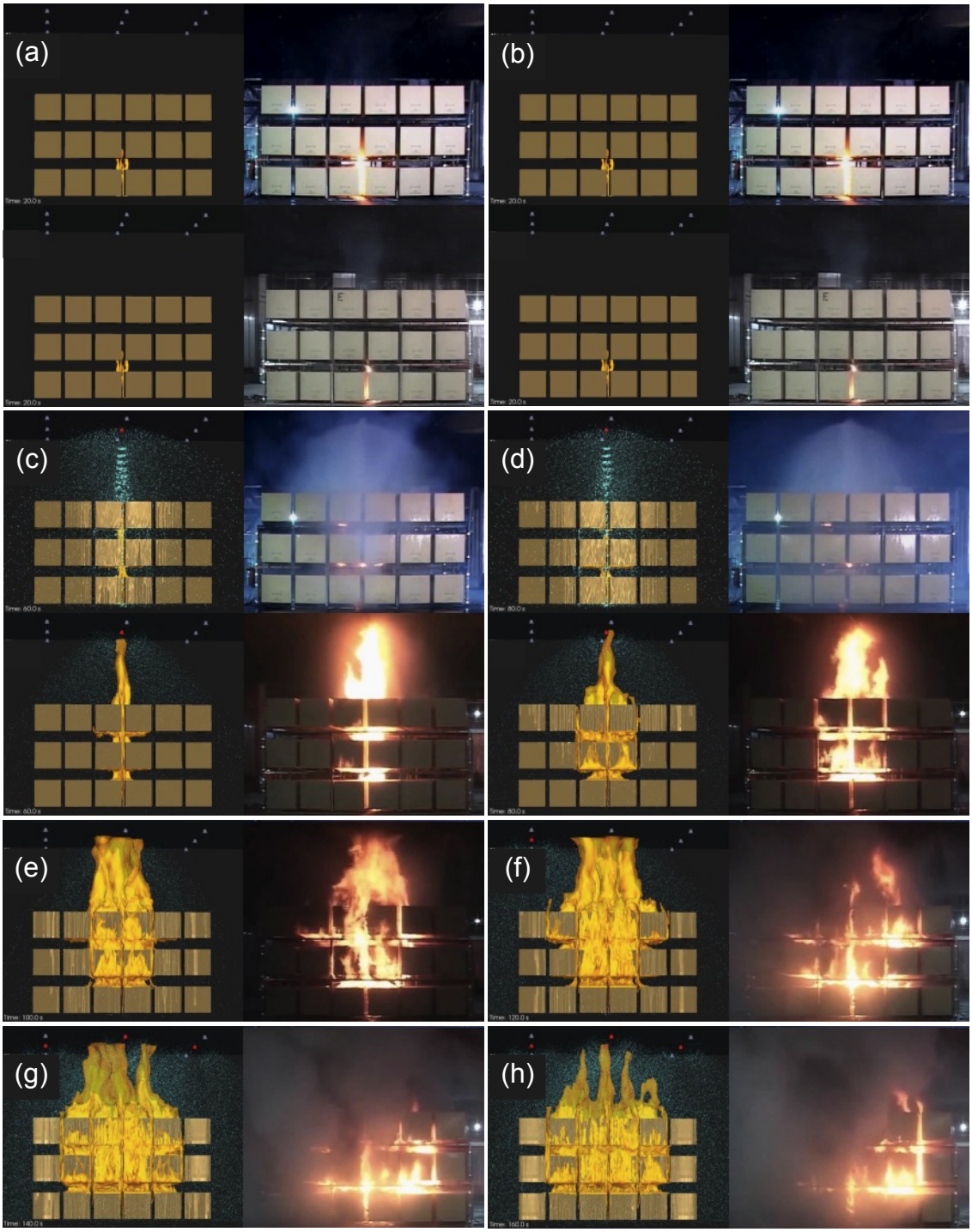

Fig. 4. Snapshots during sprinklered fire tests from (a) 20 s to (h) 160 s in 20 s increments. Left: model visualizations; right: test video images. (a-d) top: K14 sprinkler case; bottom: K11.2 case; (e-h) K11.2 case.

Table 3. Sprinkler activation time and number.

		Test 1	Test 2	Test 3	Test average	Model
K14	1st activation [s]	47	50	40	45.7	42
	number activated	1	1	1	1	1
K11.2	1st activation [s]	62	55	76	64.3	59
	2nd activation [s]	100	97	111	102.7	117
	number activated	7	5	7	6.3	5

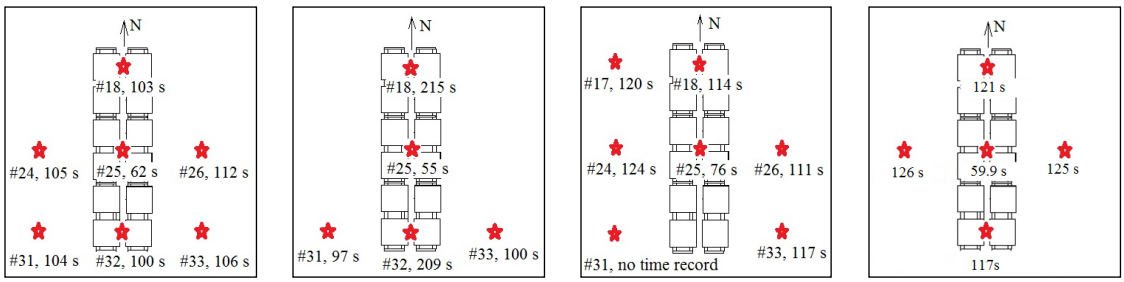

(a) Test 1 (b) Test 2 (c) Test 3 (d) Model

Fig. 5. Sprinkler activation time and location for K11.2 cases.

The randomness of later sprinkler activations and erratic activation pattern of the three repeat tests in Fig. 5 may be attributed to the well known sprinkler skipping phenomenon [30], which is not accounted for in the current model. Yet, given the variability of the tests, a statistical comparison of the sprinkler activation times may be useful. Table 4 shows the number of sprinklers active during several 50-seconds time intervals. This representation smoothes out the large variability of the large-scale sprinkler tests and allows for a more meaningful comparison with the simulation results. It is seen from Table 4 that, despite existing limitations of the model, the number of sprinklers operated within the chosen 50-seconds time intervals is within the scatter of the test data.

Table 4. Number of activated sprinklers within 50-second time intervals in K11.2 tests.

Time interval	Test 1	Test 2	Test3	Test Average	Model
0-50 s	0	0	0	0	0
50-100 s	2	1	1	1.3	1
100-150 s	7	3	6	5.3	5
150-200 s	7	3	6	5.4	5
200-250 s	7	5	7	6.3	5

Suppression Model Analysis

Following the above comparison of the model performance against experimental data, focus is now placed on extracting and analyzing "simulated measurements" that are difficult to gather in large-scale sprinklered fire testing. We first study the amount of water that penetrates the fire plume and reaches the top of the fuel array, an important quantity to characterize sprinkler's performance. This water flow density is termed Actual Delivered Density (ADD), and is usually measured under a prescribed fire source using an ADD apparatus [31] as it is not possible to measure accurately in actual large-scale fire tests.

A related study [14] has reported the measured ADD for a single K11.2 sprinkler, at 1.31 bar located on the axis of a constant fire with 2 MW convective HRR, to be 5.85 L/min/m^2 for the inner columns, and 6.41 L/min/m^2 for the intermediate columns. These steady state ADDs are compared, in Fig. 6, with the transient spatial-averaged water flux on the top of the rack from the suppression simulation. As one can see, the initial water flux for the inner and intermediate columns is close to the reported ADD value. The inner columns collect more water, while the intermediate columns collect less water than in the ADD test. The difference may come from the deficiency of the current sprinkler injection model as well as the spray transport model with coarse resolution. It can be also attributed to the difference in fire size dynamics. In the ADD tests, a heptane spray fire is created to mimic the rack storage fire. Differences exist in the fire

plume temperature and velocity, and can cause some deviations in the water distribution pattern compared to the rack storage tests. Despite some differences, the predicted overall water flux is in reasonable agreement with the ADD test data. The water flux on the outer columns is considerably reduced (2.6 L/min/m^2) compared to the other columns, indicating the extent of the coverage area of a single sprinkler head.

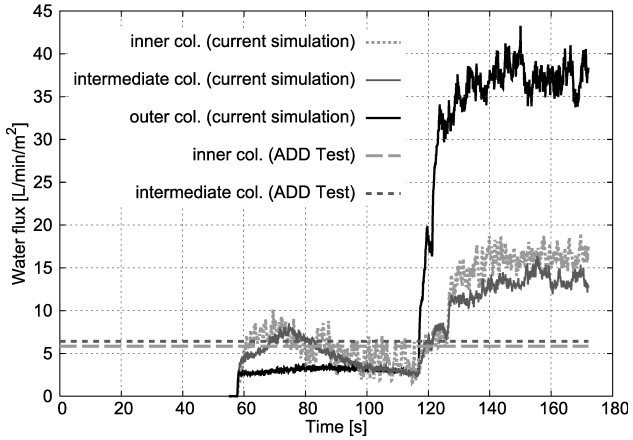

Fig. 6. Actual delivered density from the simulation for the K11.2 case.

It is observed in Fig. 6 that, immediately after the sprinkler spray is applied, from 60s to 75s, the water density in the intermediate columns has a 60% increase in water flux (from 4.8 to 7.6 L/min/m^2). It is due to the weakening of the convective flow by the water spray, although this gas phase cooling effect does not lead to a reduction in the overall chemical heat release rate. After 75 s, when the fire grows to a sufficiently large size, the water fluxes on both inner and intermediate columns start to reduce continuously until more sprinklers activate. Eventually when five sprinklers are activated, water reaches the inner columns and almost triples the flux observed during the initial stage, and there is an order of magnitude increase in the water flux on the outer columns.

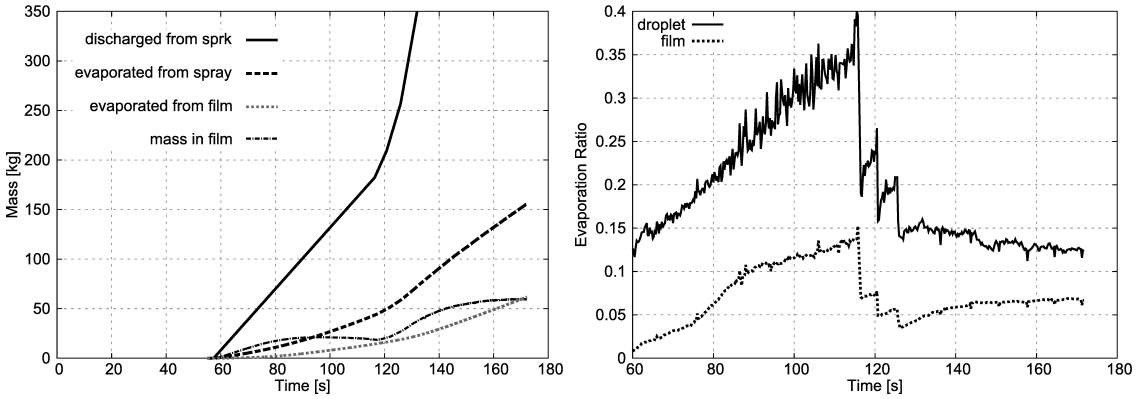

Fig. 7. Water distribution (a), and evaporation ratios from droplet and water film (b) for the K11.2 case.

Balance of water distribution is also of interest, but difficult to measure in fire tests. The simulated quantities for the K11.2 case are presented in Fig. 7a, including the cumulative water mass discharged from sprinklers, cumulative mass water evaporated from spray and film respectively, and the amount of water present as a film on the boxes. The total discharged water mass increases with a rate of 183 L/min when the first sprinkler is activated. The water in the film is about 25% of the total discharged water before 80s. During the same time, the sum of the water in the film and that evaporated from the film amounts to 28%, which is roughly the water fraction that reaches the main fuel array, assuming there is no water run off from the fuel array to the ground. The amount of water evaporated from the spray droplet is roughly triple of that evaporated from the surface water film. The total evaporated water fraction combined from both sources is about 31% before the second sprinkler activation at about 120s.

The rates of evaporation normalized by the water discharge rate are plotted in Fig. 7b as an evaporation ratio. This is a measure of the instantaneous fraction of water being evaporated. The evaporation ratio for the spray droplets increases linearly from 12% to 35% during the time period of 60-120s, and reduces back to about 15% when additional four sprinklers activate. The same quantity for the surface water film has the same trend, but remains about 1/3 of that for the spray. It is seen that, for this particular sprinkler and given fire hazard, a significant amount of water is evaporated before reaching the fuel array. This indicates ineffectiveness of the protection scheme tested for the given fire hazard.

CONCLUSION

We have presented results of CFD modeling of large-scale rack storage fires and their suppression with two types of automatic sprinklers. The results of simulations are evaluated against large-scale fire test data, which include repeat tests to characterize experimental variability. The recently developed FireFOAM code is used in the simulations. The major sub-models related to fire growth, fire suppression and sprinkler response are fully integrated in the code, making CFD modeling applicable to such a complicated multi-physics scenario. In general, it has been shown that the FireFOAM code and the modeled physics are sufficiently advanced to make meaningful modeling of sprinkler-based rack storage fire suppression possible.

In particular, the modeled fire growth rate for the free burn fire compares quantitatively well with the experimental measurements, in both the initial growth period and peak heat release rate. The suppression simulations for the two cases studied with K11.2 and K14 sprinklers adequately capture the effectiveness, or lack thereof, of the two protection systems. The predicted first sprinkler activation times are within experimental uncertainties for the two sprinkler types. In the K11.2 fire tests, large variations are present for the time and sequence of subsequent sprinkler activations. Despite the variations, the predicted second sprinkler activation time is close to the test data and, statistically, the number of sprinklers operating within 50-seconds time intervals is within the scatter of the data. The model does reproduce the main repeatable trend in the suppression phenomena that manifests itself in the tests. Furthermore, quantities that cannot be measured in the fire tests are analyzed in the current numerical study. This analysis has shown that the present CFD model can be useful to understand fire suppression phenomena, their controlling parameters and sensitivity of these parameters to variations in fire hazard and protection solutions.

Limitations remain in the models that do not allow for full representation of the physical phenomena involved in such complicated fire suppression scenarios. For example, the combustion model used in this study does not account for gas phase extinction. The attenuation of radiation by droplets and water vapor is not modeled; neither is the water's effect on soot formation/oxidation. Geometry changes and delamination of the solid fuel in fire affecting burning and water transport are not considered in the current pyrolysis model. Modeling sprinkler cooling by droplet impingement needs to be included and validated in a statistically meaningful manner. Detailed validation of the heat transfer, evaporation, and suppression models that are used in the surface film treatment is also desired. These physical effects and their modeling will be the subject of future studies, many of which need to be conducted in separate, smaller scale and better controlled conditions. On the other hand, the promising predictions from the current CFD simulations of the suppression tests confirm that the surface wetting and cooling are the controlling suppression mechanism, and other neglected physics might only play a secondary role.

Further understanding of rack storage fire suppression defines additional areas for future studies, which include, among others, numerical analysis of the effect of tier height on the fire hazard and required protection schemes. The inclusion of wood pallets to represent standard Class 2 commodity and modeling of complex fuels are also planned.

ACKNOWLEDGEMENTS

This study was funded by FM Global and performed within the framework of the FM Global Strategic Research Program on Fire Modeling. The authors thank Drs. Louis Gritzo and Robert G. Bill, Jr. for their long-term support and encouragement for this research. Sergio Ferraris, Andy Heather, Mattijs Janssens, and Henry Weller, from OpenCFD Ltd., are gratefully acknowledged for their contribution to the development of the code used in this study. OpenFOAM is a registered trademark of the OpenFOAM Foundation.

REFERENCES

[1] McGrattan, K., "Fire Modeling: Where Are We? Where Are We Going?" *Fire Safety Science -- Proceedings of the Eighth International Symposium*, International Association for Fire Safety Science, 2005, pp.: 53-68, http://dx.doi.org/10.3801/IAFSS.FSS.8-53

[2] Trouvé, A. and Wang, Y., (2010) Large Eddy Simulation of Compartment Fires, International Journal of Computational Fluid Dynamics 24: 449-466, http://dx.doi.org/10.1080/10618562.2010.541393

[3] Novozhilov, V., Harvie, D.J.E., and Kent, J.H., (1997) A Computational Fluid Dynamics Study of Wood Fire Extinguishment by Water Sprinkler, Fire Safety Journal 29: 259-282.

[4] McGrattan, K.B., Hamins, A., and Stroup, D., "Sprinkler, Smoke & Heat Vent, Draft Curtain Interaction – Large Scale Experiments and Model Development," National Institute of Standards and Technology Report NISTIR 6196-1, Gaithersburg, MD, 1998, 159 p.

[5] Rein, G., Torero, J.L., Jahn, W., Stern-Gottfried, J, Ryder N.L., Desanghere, S., Lázaro, M., Mowrer, F., Coles, A., Joyeus, D., Alvear, D., Capote, J.A., Jowsey, A., Abecassis-Empis, C., and Reszka, P., (2009) Round-robin Study of A Priori Modeling Predictions of the Dalmarnock Fire Test One, Fire Safety Journal 44: 590-602, http://dx.doi.org/10.1016/j.firesaf.2008.12.008

[6] Wang, Y., Chatterjee, P., and de Ris, J. L., (2011) Large Eddy Simulation of Fire Plumes, Proceedings of the Combustion Institute 33: 2473-2480, http://doi:10.1016/j.proci.2010.07.031

[7] Bill Jr., R.G. and Dorofeev, S.B., "An Overview of Fire Modeling at FM Global," *Proceedings of the 12th International Conference on Fire and Materials*, Interscience Communications, 2011, pp. 221-232.

[8] Weller, H.G., Tabor, G., Jasak, H., and Fureby, C., (1998) A Tensorial Approach to Computational Continuum Mechanics Using Object Oriented Techniques, Computers in Physics, 12: 620-631, http://dx.doi.org/10.1063/1.168744

[9] Wang, Y., Chatterjee, P., and de Ris, J. L., "Large Eddy Simulation of Thermal and Fire Plumes," *Proceedings of the 6th International Seminar on Fire and Explosion Hazards*, 2010, pp. 267-278, http://dx.doi.org/10.3850/978-981-08-7724-8_04-02

[10] Maragkos, G., Rauwoens, P., Wang, Y., and Merci, B., (2013) Large Eddy Simulations of the Flow in the Near-Field Region of a Turbulent Buoyant Helium Plume, Flow Turbulence and Combustion 90: 511-543, http://dx.doi.org/10.1007/s10494-012-9437-5

[11] Chatterjee, P., de Ris, J. L., Wang, Y., and Dorofeev, S. B., (2011) A Model for Soot Radiation in Buoyant Diffusion Flames, Proceedings of the Combustion Institute, 33: 2665-2671, http://doi:10.1016/ j.proci.2010.06.112

[12] Chaos, M., Khan, M.M., Krishnamoorthy, N., de Ris, J.L., and Dorofeev, S.B., (2011) Evaluation of Optimization Schemes and Determination of Solid Fuel Properties for CFD Fire Models Using Bench-Scale Pyrolysis Tests, Proceedings of the Combustion Institute, 33: 2599-2606, http://dx.doi.org/10.1016/j.proci.2010.07.018

[13] Zhou, X., D'Aniello, S.P., and Yu, H.-Z, (2012) Spray Characterization Measurements of a Pendent Fire Sprinkler, Fire Safety Journal, 54: 36-48, http://dx.doi.org/10.1016/j.firesaf.2012.07.007

[14] Meredith, K.V., Chatterjee, P., Zhou, X., Wang, Y. and Yu, H.-Z., "Validation of Spray Water Distribution Patterns for the K11.2 Sprinkler in the Presence of a Rack Storage Fire Plume Generator," *13th International Conference and Exhibition on Fire Science and Engineering*, Nr Windsor, UK, 2013.

[15] Meredith, K.V., Xin, Y., and de Vries, J., "A Numerical Model for Simulation of Thin-Film Water Transport over Solid Fuel Surfaces," *Fire Safety Science – Proceedings of the Tenth International Symposium,* International Association for Fire Safety Science, 2011, pp. 415-428, http://dx.doi.org/10.3801/IAFSS.FSS.10-415

[16] Meredith, K.V., de Vries, J., Wang, Y., and Xin, Y., (2013) A Comprehensive Model for Simulating the Interaction of Water with Solid Surfaces in Fire Suppression Environments, Proceedings of the Combustion Institute, 34: 2719-2726, http://dx.doi.org/10.1016/j.proci.2012.06.094

[17] Krishnamoorthy, N., Chaos, M., Khan, M.M., Chatterjee, P., Wang, Y., and Dorofeev, S.B., "Application of Bench-scale Material Flammability Data to Model Flame Spread in Medium Scale Parallel Panel Test," *Proceedings of the 12th International Fire Science and Engineering Conference*, Interscience Communications, 2010, pp. 709-720.

[18] Wang, Y., Chaos, M., and Dorofeev, S.B., "CFD Modeling of Flame Spread Over Corrugated Cardboard Panels," *Proceedings of 13th International Conference on Fire and Materials*, Interscience Communications, 2013, pp. 437-448.

[19] Chatterjee, P., Wang, Y., Chaos, M., Meredith, K.V., Zhou, X., and Dorofeev, S.B., "Numerical Simulation of Fire Growth on Corrugated Cardboard Commodities in Three-Tier-High Rack Storage Arrays," *Proceedings of the 13th International Conference and Exhibition on Fire Science and Engineering*, Nr Windsor, UK, 2013.

[20] Meredith, K.V., Chatterjee, P., Wang, Y., and Xin, Y., "Simulating Sprinkler Based Rack Storage Fire Suppression Under Uniform Water Application," *Proceedings of the 7th International Seminar on Fire and Explosion Hazards*, 2013, pp. 511-520, http://dx.doi.org/10.3850/978-981-07-5936-0_07-08

[21] Zeng, D., Chaos, M., Khan, M.M., and Dorofeev, S.B. "Experimental Study of Radiation Emission from Corrugated Cardboard Flames," *Proceedings of the 13th International Conference and Exhibition on Fire Science and Engineering*, Nr Windsor, UK, 2013.

[22] Ren, N., Wang, Y., Vilfayeau, S. and Trouvé, A., "Large Eddy Simulation of Propylene Turbulent Vertical Wall Fires", *Proceedings of the 7th International Seminar on Fire and Explosion Hazards*, 2013, pp. 511-520, http://dx.doi.org/10.3850/978-981-07-5936-0_04-04

[23] Quintiere, J.G., Fundamentals of Fire Phenomena, John Wiley and Sons, Chichester, 2006, p. 248.

[24] Chaos, M., Khan, M.M., and Dorofeev, S.B., (2013) Pyrolysis of Corrugated Cardboard in Inert and Oxidative Environments, Proceedings of the Combustion Institute, 34: 2583-2590, http://dx.doi.org/10.1016/j.proci.2012.06.031

[25] Heskestad, G. and Bill Jr., R.G., (1988) Quantification of Thermal Responsiveness of Automatic Sprinklers Including Conduction Effects, Fire Safety Journal, 14: 113-125.

[26] Xin, Y., de Vries, J., Meredith, K.V., Zhou, X., Thumuluru, S. and Yu, H-Z., "Fire Suppression Physics for Sprinkler Protection," *Proceedings of FIRESEAT Symposium*, Edinburgh, UK, 2011 pp. 23-36.

[27] de Vries J., Meredith K.V. and Xin, Y., "An Experimental Study of Fire Suppression Physics for Sprinkler Protection," *Fire Safety Science - Proceedings of the Tenth International Symposium, International Association for Fire Safety Science*, 2010, pp. 429-442.

[28] Novozhilov, V., (2007) Fire Suppression Studies, Thermal Science 11: 161-180, http://dx.doi.org/10.2298/TSCI0702161N

[29] Xin, Y. and Tamanini, F., "Assessment of Commodity Classification for Sprinkler Protection Using Representative Fuels," *Fire Safety Science – Proceedings of the Ninth International Symposium,* International Association for Fire Safety Science, 2009, pp. 527-538, http://dx.doi.org/10.3801/IAFSS.FSS.9-527

[30] Croce, P.A., Hill, J.P. and Xin, Y., (2005) An Investigation of the Causative Mechanism of Sprinkler Skipping, Journal of Fire Protection Engineering, 15:2.

[31] Chan, T.-S., Kung, H.-C., Yu, H.-Z., and Brown, W.R., "Experimental Study of Actual Delivered Density for Rack-Storage Fires," *Fire Safety Science – Proceedings of the Fourth International Symposium*, International Association for Fire Safety Science, 1994: 913-924.